



Hydrogen peroxide sol–gel coating of microencapsulated phase change materials by metal oxides

Alexey A. Mikhaylov¹ · Alexander G. Medvedev¹ · Dmitry A. Grishanov^{1,2} · Sergey Sladkevich² · Zhichuan J. Xu³ · Konstantin A. Sakharov³ · Sigalit Meker^{2,3} · Petr V. Prikhodchenko¹ · Ovdia Lev^{2,3}

Received: 18 February 2020 / Accepted: 22 May 2020 / Published online: 9 June 2020
© Springer Science+Business Media, LLC, part of Springer Nature 2020

Abstract

Hydrogen peroxide assisted sol–gel coating of core-shell microcapsules of phase change materials (PCMs) is reported. A doubly coated paraffin core with an inner poly(melamine-formaldehyde) shell and an outer coating of peroxostannate, peroxyantimonate, their mixture or the respective metal oxides are reported. Triple coating of the paraffin core with a poly(melamine-formaldehyde) inner shell, tin oxide middle layer and graphene oxide outer coating is also achieved by hydrogen peroxide sol–gel processing. The latent heats of the microencapsulated PCMs ranged between 122 and 192 J g⁻¹. The sol–gel process involves stabilization of the peroxostannate or peroxyantimonate sol in basic aqueous hydrogen peroxide and subsequent destabilization and deposition of the sol by addition of an antisolvent. Transformation to the metal oxide coating is conducted by chemical reduction with sodium sulfite or by mild heat treatment without leakage of the paraffin core.

✉ Petr V. Prikhodchenko
prihman@gmail.com
✉ Ovdia Lev
ovadia@mail.huji.ac.il

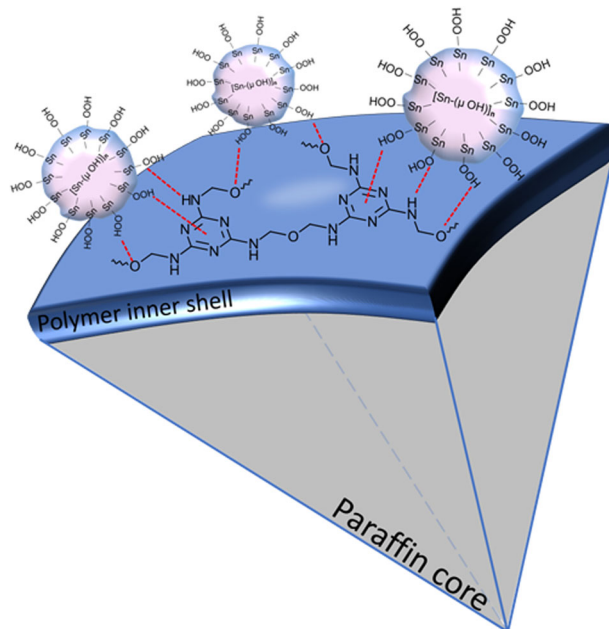
¹ Kurnakov Institute of General and Inorganic Chemistry,
Russian Academy of Sciences, Leninskii Prosp. 31,
Moscow, Russia 119991

² The Casali Center and the Institute of Chemistry and The Harvey
M. Krueger Family Center for Nanoscience and Nanotechnology,
The Hebrew University of Jerusalem, Edmond J. Safra Campus,
91904 Jerusalem, Israel

³ Singapore-HUJ Alliance for Research and Enterprise,
NEW-CREATE Phase II Campus for Research Excellence and
Technological Enterprise (CREATE) 1 CREATE Way,
Singapore 138602, Singapore

Graphical Abstract

The hydrogen bonding of hydroperoxo capped stannate nanoparticles to poly(melamine formaldehyde) - paraffin microcapsule.



Keywords Phase change materials · Heat storage · Metal oxide coating · Hydrogen peroxide sol-gel · Tin oxide · Antimony oxide

Highlights

- H_2O_2 assisted sol-gel coating of phase change organic-inorganic phase change microcapsules.
- Organic-inorganic, core-shell phase change microcapsules with up to 192 J g^{-1} latent heat.
- SnO_2 and reduced graphene oxide coating of paraffin - poly(melamine-formaldehyde) microcapsules.

1 Introduction

Storage of energy to bridge the time gap between energy availability and consumption is receiving increased attention. Energy storage is required for different time scales. The most frequently used is the storage of solar energy for night consumption, be it in power stations, home solar heaters or more complex, intermediate-scale storage of energy for solar dehumidification of air conditioning systems or for solar desalination systems. Another important class of energy conservation systems is in the field of building materials to buffer day and night temperature changes by latent heat storage materials, be they plasterboards, skim coats or even bricks. However, the time scale involved in energy conservation varies significantly and intermittent energy storage is needed for large-scale wind energy conservation and for small applications such as cold or hot food preservation. The dissipation of heat in electronic circuitry

and equipment, ranging from PC processors to large-scale data centers are required over widely different time scales. This is also true for energy storage in garments and furniture that should maintain human comfort temperature for different time spans ranging from minutes to a full day. Another important class are heat exchangers where latent heat storage can increase heat transfer rate, and again, the associated time scale can range from seconds to a few hours depending on the circulation time. Many of these tasks can be accomplished by active heat storage means, e.g. by transforming the heat and radiation into electric heat stored in batteries, however, this process involves large capital costs, energy losses due to the inherent inefficiency of power transformations, and it is affordable only for large applications.

The most useful class of phase change materials are paraffins and to some extent fatty acids, which are cheap, have a large range of melting temperatures and have

reasonably high latent heat. These come with a large drawback – low thermal conductivity and lower compatibility with hydrophilic garments, building materials and aqueous or hydrophilic thermal fluids [1–4]. This is particularly important for applications requiring fast temperature fluctuations for fast heat dissipation or prompt thermal buffering. One way to bridge over these drawbacks is to microencapsulate the paraffins in thin organic or inorganic shells. Organic shells, such as poly(melamine-formaldehyde) or poly(methylmethacrylate) provide hermetic sealing even by very thin polymeric shells, but their thermal conductivity is low, not much different from the organic core, and the incompatibility with inorganic building materials and hydrophilic fluids is not resolved. Several inorganic shells including titanium and silicon oxides were synthesized [5–7], but in order to attain hermetic sealing with zero leak of the melted paraffin, a thick shell is required, which inevitably reduces the specific latent heat of the composite. Recently, we have introduced a way to benefit from the advantages of both approaches by coating of commercially available paraffin – poly(melamine-formaldehyde) core-shell microcapsules by a thin layer of zinc peroxide using hydrogen peroxide assisted sol–gel processing [8]. The process involves sol stabilization by aqueous hydrogen peroxide solution and subsequent deposition of the nanoparticles by a controlled pH reduction, which can be achieved by slow addition of hydrogen peroxide [9–12]. In the current article, we expand the approach to obtain coating of the polymeric capsules by p-block element oxides and peroxides. The deposition of the peroxides of tin and antimony, and their mixed oxide by hydrogen peroxide assisted sol–gel processing is described in this article. Zinc is a transition metal and its peroxo coordination has more of a covalent bonding whereas the p-block element peroxides are more polar with different properties. A method for using sol–gel processing to obtain a three layered shell comprised of poly(melamine-formaldehyde), tin oxide or antimony oxide and an outer thin film of graphene oxide is introduced.

2 Experimental part

2.1 Materials

PCM microspheres, containing octadecane core encapsulated in poly(melamine-formaldehyde) shell (MCT) were purchased from Microtek Laboratories Inc. [13]. Zinc acetate dihydrate was purchased from Merck Millipore, tin (IV) chloride, antimony(V) chloride, tetramethylammonium hydroxide (25 wt% in water), sodium sulfite, ammonium hydroxide, hydrogen peroxide (30 wt%), ethanol, diethyl ether, sodium borohydride, hydrazine, potassium

peroxodisulfate, phosphorus pentoxide were purchased from Sigma-Aldrich.

2.2 Synthesis

2.2.1 ZnO coating of PCMs

154 mg of zinc acetate dihydrate were dissolved in 2 mL of concentrated 28–30 wt% aqueous ammonia. Then 5 mL of 10 wt% hydrogen peroxide solution were added and subsequently 300 mg of MCT spheres were introduced under gentle stirring for 10 min. 15 mL of 30 wt% hydrogen peroxide solution were added, slowly, drop by drop to the suspension with gentle stirring to obtain zinc peroxide precipitate on the PCM spheres. The product was separated by filtration on paper filter and washed 3 times by water and once by ethanol and then dried under vacuum for 30 min. The ZnO₂ coated PCM powder was marked as 'MCT-ZnO₂'.

We made various attempts to convert the zinc peroxide (and the other hydroperoxo films) to the respective oxide, by different chemical and physical treatments. For example, the coated microcapsules were dispersed in aqueous solution of NaBH₄ or N₂H₄ under moderate heating. Microwave treatment of the dry coated material for 5 min in 700 W oven was also attempted. However, these treatments resulted in peeling off of the inorganic coating. The most successful protocols included mild heat treatment or sulfite reduction [8]. Heat treatment was conducted at 150 °C for 3 h in argon atmosphere. Sodium sulfite reduction was carried out by dispersing 1 g of dry powder in 40 mL of 0.1 M Na₂SO₃ aqueous solution for 3 days with stirring at room temperature. The filtered and washed products are denoted by addition of -SO₃ to the notation of hydroperoxo moiety, e.g. 'MCT-ZnO₂-SO₃'.

2.2.2 Peroxostannate coated PCM microcapsules (MCT-SnOOH)

Hydroxostannate solution was prepared by dissolution of 10 mL of SnCl₄ (0.086 mol) in 20 mL of deionized water (DIW) and neutralization with ammonia until pH 7. The precipitate was washed several times with water and dissolved in 31 mL of aqueous (25 wt%) tetramethylammonium hydroxide (0.086 mol) under moderate heating. After full dissolution, water was added to achieve 1.4 M tin concentration. Then 0.7 mL of 1.4 M tetramethylammonium hydroxostannate solution was added gradually (under gentle stirring for 10 min) to 20 mL of 15 wt% H₂O₂ containing 300 mg of MCT spheres. Precipitation was accomplished by addition of 50 ml ethanol. The product was separated by filtration, washed on filter paper with water and ethanol and dried in vacuum for 30 min.

2.2.3 Peroxoantimonate coated PCM microcapsules (MCT-SbOOH)

Hydroxoantimonate solution was prepared by dissolution of 10 mL of SbCl_5 (0.078 mol) in a few mL of DIW and neutralization with ammonia until pH 7. The precipitate was washed several times with water and dissolved in 28.5 mL of aqueous (25 wt%) tetramethylammonium hydroxide (0.078 mol) under moderate heating (the dissolution process takes ~4 h). After full dissolution, water was added to achieve 1.4 M antimony concentration. Then, 0.7 mL of 1.4 M tetramethylammonium hydroxoantimonate solution was added to 20 mL 15 wt% H_2O_2 . Subsequently, 300 mg of PCM spheres were introduced under gentle stirring for 10 min. Precipitation was accomplished by the addition of 50 mL of ethanol. The product was separated by filtration, washed on filter paper with water and ethanol and then dried in vacuum for 30 min.

2.2.4 Peroxostannate-graphene oxide coating of PCMs (MCT-SnOOH-GO)

2.8 g of aqueous GO dispersion (2 wt%) were dispersed in 15 mL of hydrogen peroxide (30 wt%) by sonication. Then 0.7 mL of hydroxostannate solution (1.4 M) was added. Subsequently, 300 mg of PCM spheres were introduced under gentle stirring for 10 min. Precipitation of peroxostannate on the graphene oxide (GO) and poly(melamine-formaldehyde) surface was accomplished by addition of 60 mL of ethanol. The coated material was washed with ethanol/diethyl ether solution and dried under vacuum at room temperature.

2.2.5 Peroxoantimonate-graphene oxide coating of PCMs (MCT-SbOOH-GO)

2.8 g of aqueous GO dispersion (2 wt%) were dispersed in 15 mL of hydrogen peroxide (30 wt%) by sonication. Then 0.7 mL of hydroxoantimonate solution (1.4 M) was added. Subsequently, 300 mg of PCM spheres were introduced under gentle stirring for 10 min. Precipitation of peroxoantimonate onto the GO and microencapsulated PCM surface was accomplished by addition of 60–70 mL of ethanol. The coated material washed with the ethanol/diethylether solution and dried under vacuum at room temperature.

2.2.6 Mixed peroxoantimonate-peroxostannate coated PCM microcapsules (MCT-SnSbOOH)

0.190 mL of hydroxostannate (1.4 M) and 0.5 mL of hydroxoantimonate (1.4 M) solutions were mixed in 15 mL of hydrogen peroxide (30 wt%) with addition of 8 mL of water. Typically, 300 mg of PCMs were dispersed in 15 mL of the precursor solution by sonication, and after additional 10 min of

stirring, precipitation of particles on the PCMs surface was accomplished by addition of 120 mL of ethanol. Coated PCM was washed with ethanol and dried under vacuum at room temperature.

2.2.7 Preparation of graphene oxide

Graphene oxide (GO) was synthesized from exfoliated carbon by a modified Hummers method [14]. In a first step, graphite powder (1 g) was added to a solution of $\text{K}_2\text{S}_2\text{O}_8$ (1.67 g) and P_2O_5 (1.67 g) in 8 mL concentrated H_2SO_4 . The mixture was kept at 80 °C for 4.5 h on a hot plate. After the mixture was cooled to room temperature, it was diluted with 0.35 L of DIW and filtered. Then, the preoxidized material was washed with DIW and dried at 60–70 °C overnight. In a second step, preoxidized carbon was redispersed in 40 mL of concentrated H_2SO_4 , and the mixture was kept in an ice bath. Then, 5 g of KMnO_4 were added gradually under constant stirring to avoid overheating. The mixture was stirred at 35 °C for 2 h, and then slowly diluted with 80 mL of DIW upon cooling in the ice bath. The mixture was stirred for an additional 2 h, and then an additional 250 mL of DIW were added, followed by addition of 6 mL of 30% H_2O_2 to react with the excess permanganate. The oxidized product was filtered and washed with 100 mL HCl (1:10) to remove metal ion impurities, followed by washing with 300 mL of DIW to remove the acid.

2.3 Material characterization

2.3.1 Determination of the peroxide content

The hydrogen peroxide concentration in the aqueous solutions and the active oxygen content in solids were determined by titration with freshly prepared 0.02 N permanganate solution (permanganometry). The accuracy of the method is within 0.1–0.3% depending on the titrant volume [15].

Differential scanning calorimetry (DSC) was performed on differential scanning calorimeter, DSC 822 Mettler, Toledo and *thermogravimetric analysis (TGA)* was conducted on Thermobalance, TG50 Mettler, Toledo. All experiments were carried out at a heating rate of 5 °C min^{-1} .

2.3.2 High resolution scanning electron microscope

SEM imaging was performed using the FEI Sirion High Resolution Scanning Electron Microscope (HR SEM, Eindhoven, Holland) and NVISION 40 Scanning Electron Microscope (Carl Zeiss, Germany). Accelerating voltage was set at 5–15 kV with 5 mm working distance. Imaging was conducted using high resolution mode. Sample powder was placed on conductive carbon tape.

X-ray powder diffraction (XRD) measurements were performed on a D8 Advance Diffractometer (Bruker AXS, Karlsruhe, Germany) with a goniometer radius 280 mm with Cu K α radiation. XRD patterns were processed using DIFFRAC.SUITE software package.

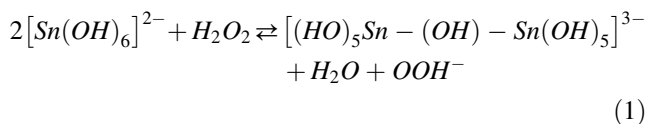
X-ray photoelectron spectroscopy (XPS) measurements were performed on a Kratos Axis Ultra X-ray photoelectron spectrometer (Manchester, UK). High resolution spectra were acquired with a monochromated Al K α (1486.6 eV) X-ray source with 0° takeoff angle. The pressure in the test chamber was maintained at $1.7 \cdot 10^{-9}$ Torr during the acquisition process. Data analysis was performed with Vision processing data reduction software (Kratos Analytical Ltd.) and CasaXPS (Casa Software Ltd.).

3 Results and discussion

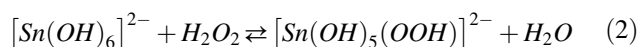
Thin film coating of PCM microcapsules is more challenging than the coating of solid particulates such as clays or carbon nanoparticles, and it demands more resources compared to the coating of flat surfaces by metal oxides. For flat surfaces, there are plenty of well-developed thin film coating techniques. Spin-, dip-, spray-, and spread-coatings and even more complicated techniques such as Langmuir-Blodgett and roll-to-roll coating have matured over the last decade or two, and they can be used to coat large flat surfaces by different oxides or mixed oxides. Moreover, low temperature variants of these techniques have already evolved to allow coating of plastics and heat sensitive materials. All these coating techniques rely on solvent evaporation to supersaturate the solution and deposit thin films on the substrate. However, none of these techniques can be used to deposit thin oxide films on particulates, since oxide concentration by evaporation will inevitably lead to aggregate formation rather than thin film deposition. Similarly, solubility change, e.g. by changing the dielectric coefficient, causes coprecipitation of a composite of the particulates and the oxide ingredient. Therefore, most of the studies on particulate coatings for the pigment and battery industries involve hydrothermal and solvothermal deposition of oxides at high temperature, usually above 100 °C or ball milling, and all of these powerful techniques are less amenable for the deposition of oxides on microencapsulated PCMs. The PCM melt may leach from the capsule to the solvent at high processing temperatures, and aggregate formation is another limitation. The Pechini process [16–19], involving complexation of the inorganic moiety by carboxylates, polymerization and subsequent heat treatment to remove the organic polymer is often used to obtain thin film coatings, but, again, the high temperature treatment is incompatible with microencapsulated PCMs. Therefore, in this article, we pursue sol-gel deposition of hydroperoxo nanoparticles from aqueous hydrogen peroxide solutions. The principle of the hydrogen peroxide sol-gel

deposition process has already been reported for the coating of oxygen containing surfaces such as aluminosilicate platelets and graphene oxide as well as acid sensitive matrices [20]. The process involves hydroxo sol formation from the aqueous salts of the elements by addition of basic solutions followed by the addition of hydrogen peroxide, which induces pH reduction and hydroperoxo sol formation. Then, further reduction of the pH and/or addition of an antisolvent such as alcohol or diethyl ether or introduction of cations forming less soluble forms like ammonia [21, 22] or sodium [10, 11] deposit the peroxy moieties exclusively on the particulates surface. Hydroperoxo functionalities are excellent hydrogen donors (compared to e.g. hydroxo functionalities [22]), and they tend to form H-bonds with oxygenated surfaces and to a somewhat lower extent also with aromatic and N-containing functionalities such as those present in the melamine-formaldehyde copolymers. This can be demonstrated by hydrogen bonding to gamma-AIOOH surfaces and hydrogen bond formation in the crystal structures of triphenylsilicon and triphenylgermanium hydroperoxides [22], hydroperoxostannate [23], as well as in the persolvates of amino acids [24] and peptides [25]. The interaction with melamine-formaldehyde copolymer is not entirely surprising, since melamine peroxosolvate has already been reported [22]. In the first part of this section, we demonstrate the formation of thin peroxy films of tin and antimony and their mixture on poly (melamine-formaldehyde) microcapsules and a comparison of these with zinc peroxide thin film coatings that have recently been introduced [8]. Subsequently, we describe how the protocol can lead to the deposition of graphene oxide on core-shell PCM microcapsules.

The deposition of peroxostannate (and peroxyantimonate and the respective peroxide) share some common features with the deposition of zinc peroxide. In all cases, that first stage involves attaining high pH in order to benefit from the high solubility of zinc and tin hydroxides. The minimum solubility of the former is around pH 7.4 [27] and the solubility of the latter is minimal at 4.5. [11]. In both cases, the pH is lowered by the introduction of hydrogen peroxide which act as an acid (Eq. (1)) and also exchanges the hydroxo ligands by hydroperoxo ligands (e.g. Eq. (2)).



and



For tin and antimony, lowering of the pH results in polycondensation, yielding nanoparticles coated by hydroperoxo groups. The acidity of hydroperoxo moieties is

much higher than hydroxo functional groups. For example, the pKa of hydrogen peroxide, 11.6 is much lower than the pKa of water, 14. Thus, the hydroperoxo nanoparticles are stabilized by the negatively charged shell of SnOO⁻ moieties, much like the stabilization of silicate nanoparticles by deprotonated silanols above the point of zero charge. The deposition of peroxyantimonate and peroxyantimonate and the respective peroxide differs somewhat from the previously reported deposition of zinc peroxide on poly(melamine-formaldehyde) shells. First, whereas the deposition of the zinc peroxide could be accomplished by a dropwise addition of aqueous hydrogen peroxide solution, the deposition of the antimony and tin hydroperoxo sols had to be conducted by the addition of ethanol as an antisolvent, which is unfortunately less environmentally friendly. We used ethanol rather than a more hydrophobic antisolvent in order to minimize extraction and loss of the paraffin from the PCM capsules. Second, whereas the deposition of the d¹⁰ element gave a crystalline zinc peroxide deposit, tin and antimony hydroperoxo deposits were amorphous. Third, the deposits of peroxyantimonate and peroxyantimonate (Fig. 1c–f) were less uniform compared to the deposit of zinc peroxide on poly(melamine-formaldehyde), though the local roughness of the zinc dioxide deposit (Fig. 1i, j) was larger due to the larger grains of zinc peroxide. The different morphologies of the zinc peroxide and the peroxyantimonate and peroxyantimonate deposits can be seen in Fig. 1 which shows SEM micrographs taken in back-scattering mode and compares the micrographs of poly(melamine-formaldehyde) encapsulated PCMs (1a,b) with the doubly coated PCMs.

The hydrogen bonding of the hydroperoxostannate capped nanoparticles is sketched in Fig. 2. The sketch shows that surface hydroperoxo groups can act both as hydrogen donors by the interaction with amide oxygen and the aromatic ring of the poly(melamine-formaldehyde) or as an H-acceptor by the interaction with the NH functionalities. Notably, all these interactions are expected to be much less energetic compared with the previously reported interactions of the hydroperoxostannate particles with oxygen hydrogen acceptors on graphene oxide [10, 11, 27], since hydroperoxo groups are stronger hydrogen donors and oxygen atoms are better hydrogen acceptors than nitrogen atoms [28].

Since, peroxy moieties exhibit low stability after long exposure to ambient conditions, and since the coexistence of peroxides and organic compounds is undesirable for safety reasons [15], the peroxy films had to be converted to the respective oxide. Several protocols were tested in order to convert the peroxy coating to the respective oxide including microwave treatment, heat treatment at different temperatures and reduction by hydrazine, sodium borohydride, and sodium sulfite. The most promising treatments involved either heat treatment at 150 °C for 3 h or immersion in stirred 0.1 M sodium sulfite for 3 days at room temperature.

Elemental analysis based on energy-dispersive X-ray spectroscopy (EDS), permanganometric titration of the peroxide coated PCMs, XPS and DSC are presented in Table 1. Since, at low concentrations of antimony and tin, it was not possible to resolve their EDS peaks, we quantified the sum of antimony and tin content together and evaluated the ratio

Fig. 1 SEM micrographs of bare commercial core-shell microcapsules comprised of paraffin core and poly(melamine-formaldehyde) shell coated without external metal oxide coating (a, b) by c, d peroxyantimonate (MCT-SnOOH); e, f peroxyantimonate (MCT-SbOOH); g, h mixed peroxyantimonate and peroxyantimonate (MCT-SnSbOOH); i, j zinc peroxide (MCT-ZnO₂); k, l MCT-SnOOH-SO₃; m, n MCT-SnOOH-GO. Two magnifications are presented for each sample

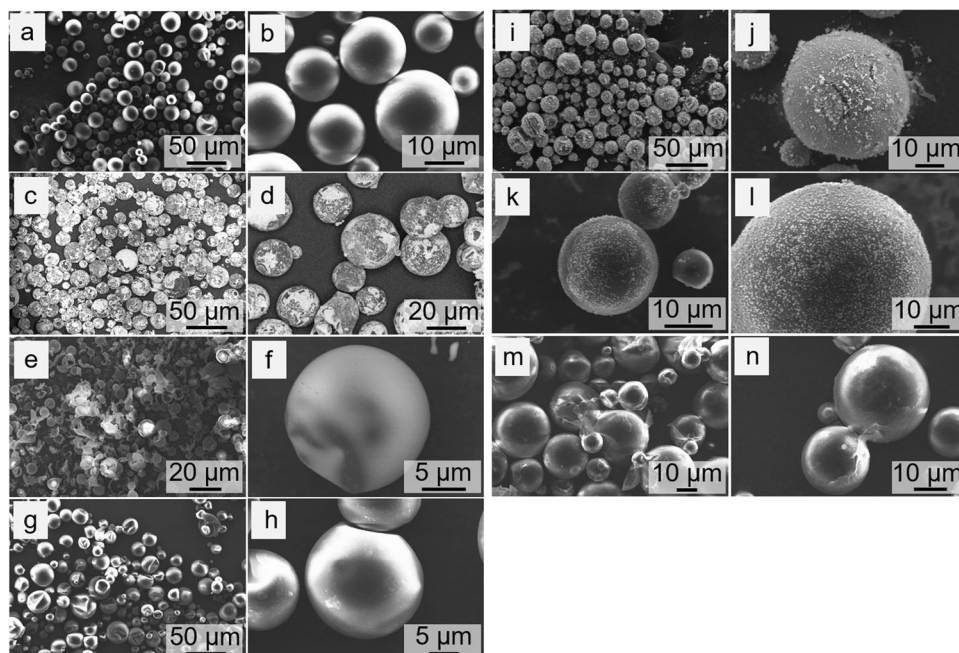
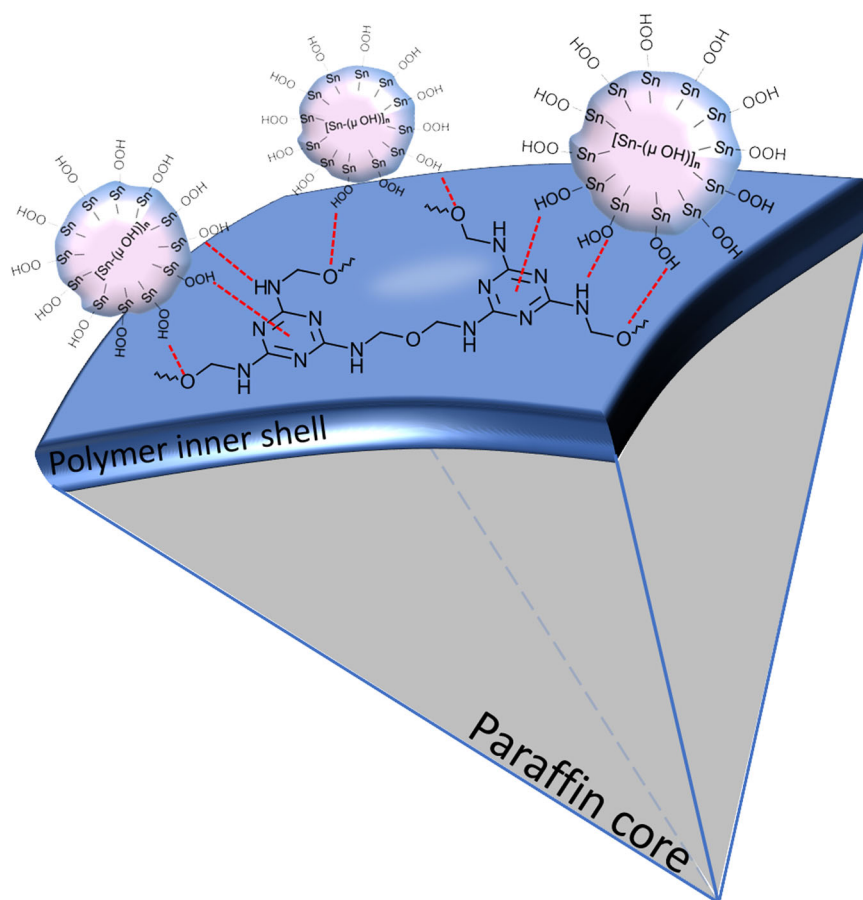


Fig. 2 The interaction of hydroperoxy capped stannate nanoparticles with poly (melamine formaldehyde) - paraffin microcapsule



between them by XPS. The XPS intensity coefficients of Sn and Sb differ by 4% only, and therefore this procedure introduces an error of only up to 4% in the determination of the antimony or tin content in mixed Sn/Sb oxide coatings.

The active oxygen content was found to prevail at relatively low concentration in all the peroxo-composites (<0.25 at%), in accordance with its role as a capping agent rather than in the skeletons of the hydroperoxy shells. Complete removal of the peroxide from MCT-SnOOH, MCT-SbOOH and MCT-SnSbOOH was observed after the chemical and thermal treatments as verified by permanganometric titration. However, some residual peroxide was retained in the zinc peroxide sample after the heat treatment at 150 °C. Increasing the treatment duration to 4 h distorted some of the PCM microcapsules as did higher temperature treatments.

The ratio between the nitrogen element which is contributed almost solely by the poly(melamine-formaldehyde) shell and the carbon element which is prevalent in the paraffin is very high, and this is attributed to the large size of the capsules relative to the low penetration depth of the X-ray. Likewise, the tin and antimony contents were overestimated due to their location in the outer shell of the doubly coated microcapsules. A better way to estimate the paraffin content in the doubly coated paraffin capsules is by

quantification of the observed latent heat of the microcapsules as measured by DSC

It was demonstrated [29, 30] that paraffin phases confined in mesoporous and nanoporous materials undergo depression of the melting point, which result in flatter DSC peaks and lower observed latent energy compared to unconfined paraffin. However, for 10 μm core microcapsules with <0.2 μm shell, the volume of the nanoconfined paraffin phase in the capsule is small, and therefore its effect on the total observed latent heat is well within our experimental error. It was demonstrated that for large pores, larger than 300 nm, the change in the melting point is <1 K. [29].

The latent heats for melting and solidification were determined by DSC and depicted as percent of the latent heat of pure octadecane (256 J g⁻¹). These values which provide a good estimate for the paraffin content in the composite are depicted in the last column of Table 1. The latent heat ranged between 50–70% of the theoretical level of pure paraffin. For comparison, for zinc dioxide the corresponding percentage is 50.4 wt%.

In order to estimate the inorganic fraction of the coating we carried out thermogravimetric analysis in nitrogen atmosphere of the tin and antimony coated material and compared them to the thermogram of the uncoated PCM

Table 1 Elemental analysis of doubly encapsulated paraffin PCMs: MCT-SnOOH, MCT-SbOOH, MCT-SnSbOOH and MCT-ZnO₂ before and after chemical and thermal transformations

Sample name	C wt% (at%) ^a	N wt% (at%) ^a	O wt% (at%) ^a	Sn wt% (at%) ^a	Sb wt% (at%) ^a	Zn wt% (at%) ^a	Active oxygen wt% ^b	Paraffin wt% ^c (by DSC: heating/cooling)
Peroxostannate coated PCMs <i>MCT-SnOOH</i>	62.5 (72.7)	25.6 (24.0)	9.3 (7.6)	2.56 (0.28)	–	–	0.16	70.6/76.3
Peroxostannate coated PCMs after sulfite reduction <i>MCT-SnOOH-SO₃</i>	65.8 (70.8)	24.7 (22.8)	7.7 (6.2)	1.79 (0.19)	–	–	NA ^d	74.9/82.1
Peroxostannate coated PCMs, after heat treatment at 150 °C <i>MCT-SnOOH-150C</i>	63.6 (69.5)	23.2 (21.7)	10.3 (8.4)	2.91 (0.32)	–	–	NA	64.8/72.0
Peroxoantimonate coated PCMs <i>MCT-SbOOH</i>	66.1 (71.7)	15.1 (14.0)	17.3 (14.1)	–	1.43 (0.15)	–	0.19	74.2/78.5
Peroxoantimonate coated PCMs after sulfite reduction <i>MCT-SbOOH-SO₃</i>	63.8 (68.5)	23.2 (21.3)	12.6 (10.1)	–	0.49 (0.05)	–	NA	70.4/77.1
Peroxoantimonate coated PCMs after heat treatment at 150 °C <i>MCT-SbOOH-150C</i>	64.1 (69.8)	19.9 (18.6)	13.9 (11.4)	–	2.00 (0.21)	–	NA	67.7/72.0
Mixed peroxoantimonate-peroxostannate coated PCMs <i>MCT-SnSbOOH</i>	67.3 (74.4)	9.7 (9.2)	19.4 (16.1)	1.8 (0.2)	1.7 (0.19)	–	0.25	56.3/63.3
Mixed peroxoantimonate-peroxostannate coated PCMs after sulfite reduction <i>MCT-SnSbOOH-SO₃</i>	69.7 (76.0)	9.9 (9.2)	17.7 (14.5)	2.6 (0.29)	0.09 (0.01)	–	NA	47.8/61.1
Mixed peroxoantimonate-peroxostannate coated PCMs after heat treatment at 150 °C <i>MCT-SnSbOOH-150C</i>	71.9 (77.8)	4.5 (4.2)	22.0 (17.9)	0.9 (0.1)	0.7 (0.07)	–	NA	56.1/63.3
Zinc peroxide coated PCMs <i>MCT-ZnO₂</i>	62.4 (66.9)	22.1 (21.2)	9.0 (7.5)	–	–	6.4 (1.3)	2.5	50.4/–60/64
Peroxostannate-graphene oxide coated PCMs <i>MCT-SnOOH-GO</i>	68.23 (72.73)	24.87 (22.73)	5.5 (4.40)	1.4 (0.15)	–	–	–	–

^aC, N, O, Sn, Sb and Zn contents are estimated by EDS^bActive oxygen content is estimated by permanganometric titration^cParaffin percentage is obtained from DSC data^dNA denotes < 0.05%

microcapsules. Figure 3 shows that residual solid at 800 °C is only 6.2% compared to 1.5% for the uncoated PCM capsule. Thus, according to this estimate the tin element constitutes ~3.7 wt% of the PCM weight, slightly more than the 3 wt% estimate based on the elemental analysis. As can be observed in Fig. 3 the antimony content cannot be calculated by a similar way since antimony oxide evaporated at high temperature.

All the XRD diffractograms of the hydroperoxo coated PCM microcapsules reveal the crystalline peaks of n-octadecane at the range $2\theta = 20\text{--}25^\circ$, whereas the zinc peroxide coated PCMs revealed an additional crystalline diffractogram (see Ref. [8]) corresponding to cubic ZnO₂ (PDF 00-013-0311). The diffractogram of the crystalline paraffin was indifferent to the coating material even after peroxide removal. Figure 4 presents the case of tin oxide coated MCT. For the samples MCT-SnOOH, MCT-SnOOH-150C and MCT-SnOOH-SO₃ corresponding to the doubly coated paraffin microcapsules before peroxide

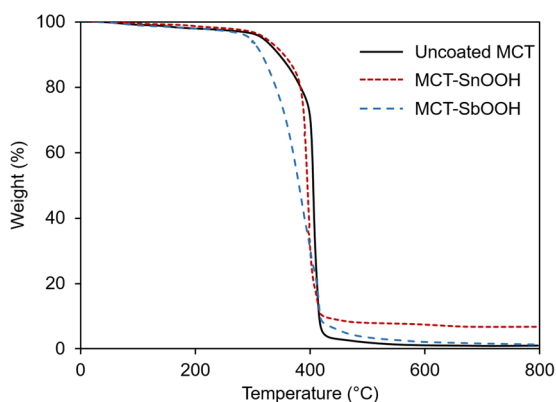


Fig. 3 TGA of doubly coated PCMs: **a** uncoated MCT, **b** MCT-SnOOH, **c** MCT-SbOOH

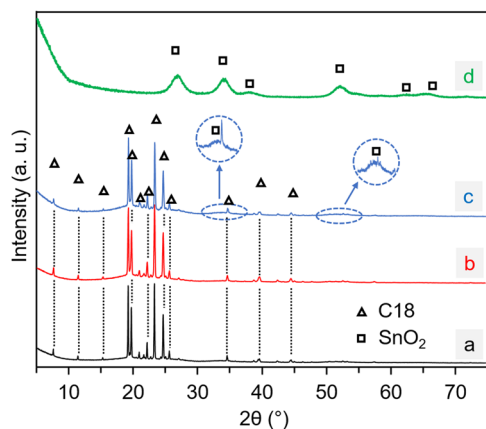


Fig. 4 XRD diffractograms of doubly coated PCMs: **a** MCT-SnOOH, **b** MCT-SnOOH-SO₃, **c** MCT-SnOOH-150C, **d** MCT-SnOOH-500C and library XRD patterns of cassiterite SnO₂ (squares) and n-octadecane (triangles)

removal, after heat treatment at 150 °C for 3 h under argon atmosphere, and after sodium sulfite reduction, only the diffraction of the crystalline paraffin is observable, and at 150 °C a shallow broad SnO₂ signal appears in the diffractogram. Heat treatment (under Ar) at 500 °C evaporates the paraffin and only the diffraction pattern of cassiterite tin dioxide (PDF 01-071-0652) is observed (with Scherrer crystalline size of 37 nm).

The diffractograms of peroxyantimonate coated PCMs (MCT-SbOOH) (Fig. 5) and mixed peroxyantimonate-peroxyantimonate coated (MCT-SnSbOOH) (Fig. 6) and their reduced and heat treated forms follow a similar pattern. In all the samples, except for the 500 °C treated samples (curves 4d and 5d) the crystalline pattern of the paraffin dominates (with the exception of the appearance of a small sodium hydroxoantimonate peak after sodium sulfite reduction of the MCT-SbOOH), and the diffraction pattern

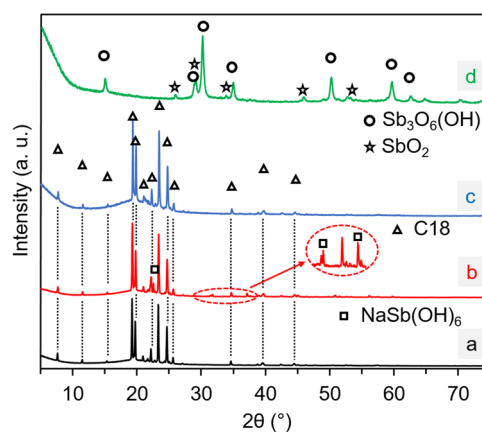


Fig. 5 XRD diffractograms of doubly coated PCMs: **a** MCT-SbOOH, **b** MCT-SbOOH-SO₃, **c** MCT-SbOOH-150C, **d** MCT-SbOOH-500C and library XRD patterns of NaSb(OH)₆ (squares), Sb₃O₆(OH) (circles), SbO₂ (stars) and n-octadecane (triangles)

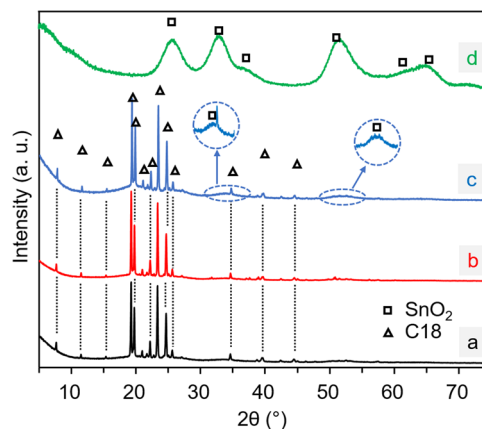


Fig. 6 XRD diffractograms of doubly coated PCMs: **a** MCT-SnSbOOH, **b** MCT-SnSbOOH-SO₃, **c** MCT-SnSbOOH-150C, **d** MCT-SnSbOOH-500C and library XRD patterns of cassiterite SnO₂ (squares) and n-octadecane (triangles)

of the paraffin is replaced by the crystalline form of Sb_3O_6 (OH) and SbO_2 (a mixed oxide phase of Sb(V) and Sb(III)) for MCT-SbOOH and by SnO_2 for heat treated MCT-SnSbOOH. The antimony oxide has probably evaporated by the prolonged heat treatment at 500 °C. The transformations of the MCT-ZnO₂ sample differed from the p-block element peroxides. ZnO_2 was transformed to hexagonal zincite, ZnO after heat treatment or chemical treatment with sodium sulfite (see ref. [8]).

3.1 Graphene oxide coated microcapsules

Graphene oxide (GO) is frequently added to improve the properties of phase change materials [31–34] due to the high thermal conductivity of reduced graphene oxide (rGO) [31]. Coating of the PCM microcapsules by an outer layer of rGO is desirable due to the direct contact of the rGO with the microcapsule [27]. Since our attempts to conduct the graphene oxide deposition directly on the poly(melamine-formaldehyde) shell were proven unsuccessful we resorted to the coating of the poly(melamine-formaldehyde) PCM microcapsules by a hydroperoxostannate intermediate layer. In this multilayer structure, the hydroperoxo capped nanoparticles form a thin film on the graphene oxide due to the efficient hydrogen bonding of hydroperoxo H-donors to the H-acceptor oxygen containing functionalities on the graphene oxide (e.g. carbonyls, epoxides, alcohols and carboxylates). The other side of the hydroperoxo nanoparticles attach efficiently to the poly(melamine-formaldehyde) shells as illustrated in Fig. 2. The coating protocol was rather simple, GO was dispersed in hydrogen peroxide and then hydroxostannate solution was added to form the GO coated by hydroperoxostannate moieties. Then, precipitation of coated GO and poly(melamine-formaldehyde) surface was accomplished by addition of ethanol antisolvent. The very same protocol worked well for the peroxyantimonate intermediate layer as well. Figure 7 depicts the

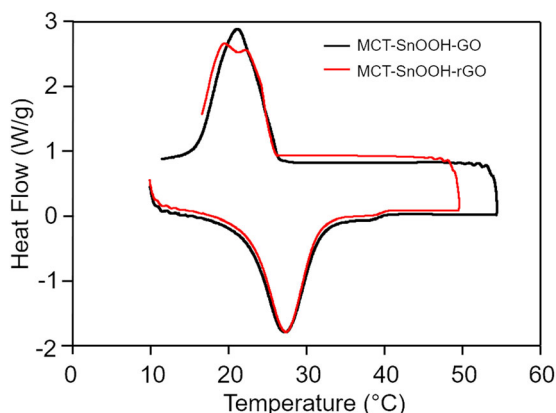


Fig. 7 DSC thermogram of triple coated, poly(melamine – formaldehyde), tin oxide, rGO before (a) and after reduction

DSC thermograms of the triple coated PCM microcapsules, MCT-SnOOH-GO before and after reduction. The paraffin content in the triple coated (poly(melamine-formaldehyde), SnOOH, GO (last row in Table 1) is only slightly smaller than peroxyantimonate and peroxyantimonate coated microcapsules (64 compared to 76 and 78 wt%).

4 Conclusions

Hydrogen peroxide sol-gel chemistry provides a promising way to deposit hydroperoxo moieties on oxygen and nitrogen containing surfaces due to the propensity to form hydroperoxo functionalities on oxide sols. These surface hydroperoxo groups can then interact strongly with oxygen and nitrogen containing surfaces due to the greater propensity of hydroperoxo groups to donate hydrogen and to participate in hydrogen bonding compared to the respective hydroxo functionalities. This feature becomes especially useful whenever coating under delicate conditions is required. In this article, this is exploited in the coating of organic PCM microcapsules by thin films of antimony and tin oxides and their respective mixed oxide, without distorting the capsules or loss of its paraffin content. Since the sol capping agent is hydrogen peroxide (in the form of hydroperoxo groups and their deprotonated forms) it can be removed under rather delicate conditions. The triple coating of poly(melamine-formaldehyde) by peroxyantimonate followed by deposition of rGO exhibits bonding of the peroxyantimonate nanoparticles to the organic moieties on the one side and to oxygen containing species of the rGO on their other side. Unlike all other nanoparticle capping agents, hydrogen peroxide can be removed completely without generating waste and without leaving a trace in the final (doubly and triply encapsulated PCM) product.

Acknowledgements This research was supported by a grant from the National Research Foundation, Prime Minister Office, Singapore under its Campus of Research Excellence and Technological Enterprise (CREATE) programme. The financial support of the Ministry of Science is thankfully acknowledged. The authors thank the Harvey M. Krueger Family Centre for Nanoscience and Nanotechnology of the Hebrew University of Jerusalem and the Israel Science Foundation (grant number 1215/19). We thank the Russian Foundation for Basic Research (grant 18-29-19119, 18-33-20211). The User Facilities Center of IGIC RAS within the State Assignment on Fundamental Research to the Kurnakov Institute of General and Inorganic Chemistry are acknowledged.

Compliance with ethical standards

Conflict of interest The authors declare that they have no conflict of interest.

Publisher's note Springer Nature remains neutral with regard to jurisdictional claims in published maps and institutional affiliations.

References

- Liu LK, Su D, Tang YJ, Fang GY (2016) Thermal conductivity enhancement of phase change materials for thermal energy storage: a review. *Renew Sustain Energy Rev* 62:305–317
- Sharma RK, Ganesan P, Tyagi VV, Metselaar HSC, Sandaran SC (2015) Developments in organic solid-liquid phase change materials and their applications in thermal energy storage. *Energy Convers Manag* 95:193–228
- Khan Z, Khan Z, Ghafoor A (2016) A review of performance enhancement of PCM based latent heat storage system within the context of materials, thermal stability and compatibility. *Energy Convers Manag* 115:132–158
- Qureshi ZA, Ali HM, Khushnood S (2018) Recent advances on thermal conductivity enhancement of phase change materials for energy storage system: a review. *Int J Heat Mass Transf* 127:838–856
- Li BX, Liu TX, Hu LY, Wang YF, Gao LN (2013) Fabrication and properties of microencapsulated paraffin@SiO₂ phase change composite for thermal energy storage. *ACS Sustain Chem Eng* 1:374–380
- Jung Y, Youm JO, Youm KH (2015) Synthesis of mono-dispersed paraffin microcapsules by polycondensation using membrane emulsification and their latent heat properties. *Macromol Res* 23:1004–1011
- Cao L, Tang F, Fang GY (2014) Synthesis and characterization of microencapsulated paraffin with titanium dioxide shell as shape-stabilized thermal energy storage materials in buildings. *Energy Build* 72:31–37
- Mikhaylov AA, Medvedev AG, Grishanov DA, Sladkevich S, Xu ZJ, Hua YE, Prikhodchenko PV, Lev O (2019) Doubly coated, organic – inorganic paraffin phase change materials: zinc oxide coating of hermetically encapsulated paraffins. *Adv Mater Interfaces* 6:1900368
- Medvedev AG, Mikhaylov AA, Grishanov DA, Yu DYW, Gun J, Sladkevich S, Lev O, Prikhodchenko PV (2017) GeO₂ thin film deposition on graphene oxide by the hydrogen peroxide route: evaluation for lithium-ion battery anode. *ACS Appl Mater Interfaces* 9:9152–9160
- Mikhaylov AA, Medvedev AG, Mason CW, Nagasubramanian A, Madhavi S, Batabyal SK, Zhang Q, Gun J, Prikhodchenko PV, Lev O (2015) Graphene oxide supported sodium stannate lithium ion battery anodes by the peroxide route: low temperature and no waste processing. *J Mater Chem A* 3:20681–20689
- Mikhaylov AA, Medvedev AG, Tripol'skaya TA, Popov VS, Mokrushin AS, Krut'ko DP, Prikhodchenko PV, Lev O (2017) H₂O₂ induced formation of graded composition sodium-doped tin dioxide and template-free synthesis of yolk-shell SnO₂ particles and their sensing application. *Dalton Trans* 46:16171–16179
- Grishanov DA, Mikhaylov AA, Medvedev AG, Gun J, Nagasubramanian A, Srinivasan M, Lev O, Prikhodchenko PV (2018) Synthesis of high volumetric capacity graphene oxide-supported tellurantimony Na- and Li-ion battery anodes by hydrogen peroxide sol gel processing. *J Colloid Interface Sci* 512:165–171
- Microtek Laboratories, Inc. <https://www.microteklabs.com/>
- Zhou X, Huang X, Qi X, Wu S, Xue C, Boey FYC, Yan Q, Chen P, Zhang H (2009) In situ synthesis of metal nanoparticles on single-layer graphene oxide and reduced graphene oxide surfaces. *J Phys Chem C* 113:10842–10846
- Schumb WC, Satterfield CN, Wentworth RP (1955) Hydrogen peroxide. Reinhold Publishing Corp, New York, NY
- Pechini MP (1967) Method of preparing lead and alkaline earth titanates and niobates and coating method using the same to form a capacitor, US Patent 3330697
- Bernardi MIB, Soledade LE, Santos IA, Leite ER, Longo E, Varela JA (2002) Influence of the concentration of Sb₂O₃ and the viscosity of the precursor solution on the electrical and optical properties of SnO₂ thin films produced by the Pechini method. *Thin Solid Films* 405:228–233
- Bernardi MIB, Feitosa CAC, Paskocimas CA, Longo E, Paiva-Santos CO (2009) Development of metal oxide nanoparticles by soft chemical method. *Ceram Int* 35:463–466
- Sladkevich S, Kyi N, Gun J, Prikhodchenko P, Ischuk S, Lev O (2011) Antimony doped tin oxide coating of muscovite clays by the Pechini route. *Thin Solid Films* 520:152–158
- Sladkevich S, Mikhaylov AA, Prikhodchenko PV, Tripol'skaya TA, Lev O (2010) Antimony tin oxide (ATO) nanoparticle formation from H₂O₂ solutions: a new generic film coating from basic solutions. *Inorg Chem* 49:9110–9112
- Mikhaylov AA, Medvedev AG, Grishanov DA, Edison E, Madhavi S, Sladkevich S, Gun J, Prikhodchenko PV, Lev O (2020) Green synthesis of a nanocrystalline tin disulfide reduced grapheneoxide anode from ammonium peroxostannate: a highlystable sodium-ion battery anode *ACS Sustain Chem Eng* 8:5485–5494
- Grishanov DA, Churakov AV, Medvedev AG, Mikhaylov AA, Lev O, Prikhodchenko PV (2019) Crystalline ammonium peroxogermanate as a waste-free, fully recyclable versatile precursor for germanium compounds. *Inorg Chem* 58:1905–1911
- Medvedev AG, Grishanov DA, Churakov AV, Mikhaylov AA, Lev O, Prikhodchenko PV (2020) Hydroperoxo double hydrogen bonding: stabilization of hydroperoxo complexes exemplified by triphenylsilicon and triphenylgermanium hydroperoxides *Cryst Eng Comm* 22:1922–1928
- Churakov AV, Sladkevich S, Lev O, Tripol'skaya TA, Prikhodchenko PV (2010) Cesium hydroperoxostannate: first complete structural characterization of a homoleptic hydroperoxocomplex. *Inorg Chem* 49:4762–4764
- Vener MV, Medvedev AG, Churakov AV, Prikhodchenko PV, Tripol'skaya TA, Lev O (2011) H-bond network in amino acid cocrystals with H₂O or H₂O₂. The DFT study of serine-H₂O and serine-H₂O₂. *J Phys Chem A* 115:13657–136663
- Churakov AV, Grishanov DA, Medvedev AG, Mikhaylov AA, Tripol'skaya TA, Vener MV, Navasardyan MA, Lev O, Prikhodchenko PV (2019) Cyclic dipeptide peroxosolvates: first direct evidence for hydrogen bonding between hydrogen peroxide and a peptide backbone. *CrystEngComm* 21:4961–4968
- Bénézech P, Palmer DA, Wesolowski DJ, Xiao C (2002) New measurements of the solubility of zinc oxide from 150 to 350 °C. *J Solut Chem* 31:947–973
- Chernyshov IYU, Vener MV, Prikhodchenko PV, Medvedev AG, Lev O, Churakov AV (2017) Peroxosolvates: formation criteria, H₂O₂ hydrogen bonding, and isomorphism with the corresponding hydrates. *Cryst Growth Des* 17:214–220
- Wang D, Sui J, Qi D, Deng S, Wei Y, Wang X, Lan X (2019) Phase transition of docosane in nanopores. *J Therm Anal Calorim* 135:2869–2877
- Jiang Q, Ward MD (2014) Crystallization under nanoscale confinement. *Chem Soc Rev* 43:2066–2079
- Huang X, Yin ZY, Wu SX, Qi XY, He QY, Zhang QC, Yan QY, Boey F, Zhang H (2011) Graphene-based materials: synthesis, characterization, properties, and applications. *Small* 7:1876–1902
- Kashyap S, Kabra S, Kandasubramanian B (2000) Graphene aerogel-based phase changing composites for thermal energy storage systems. *J Mater Sci* 55:4127–4156

33. Wu HY, Li ST, Shao YW, Jin XZ, Qi XD, Yang JH, Zhou ZW, Wang Y (2020) Melamine foam/reduced graphene oxide supported form-stable phase change materials with simultaneous shape memory property and light-to-thermal energy storage capability. *Chem Eng J* 379:122373
34. Akhiani AR, Mehrali M, Latibari ST, Mehrali M, Mahlia TMI, Sadeghinezhad E, Metselaar HSC (2015) One-step preparation of form-stable phase change material through self-assembly of fatty acid and graphene. *J Phys Chem C* 119:22787–22796